Journal of
Polymer Materials

Tech Science Press

https://doi.org/10.32604/jpm.2026.080324

ARTICLE

Internal Microstructure and Properties of a Reduced Graphene Oxide/Carbon Fiber/Carbon Based Composite Materials

Mingwei Ren[1,2], Xiangchi Hou[3], Xinyang Peng[3], Yujing Zhou[1], Kewei Gao[2], Yunbo Chen[1,*], Hong Qiu[3], Hua Bai[3] and Xiaolan Hu[3,*]

[1]Beijing National Innovation Institute of Lightweight Ltd., Beijing, China
[2]School of Materials Science and Engineering, University of Science and Technology Beijing, Beijing, China
[3]College of Materials, Xiamen University, Xiamen, China

*Corresponding Authors: Yunbo Chen. Email: chenyb@camtc.com.cn; Xiaolan Hu. Email: xlhu@xmu.edu.cn

Received: 06 February 2026; Accepted: 09 May 2026; Published: 30 June 2026

ABSTRACT: During the preparation of carbon fiber reinforced carbon matrix (C/C) composites from resin based precursors, the glassy carbon derived from resin pyrolysis is difficult to graphitize into an ordered structure during carbonization and graphitization, which adversely affects the performance of C/C composites. To enhance the transformation of resin-derived carbon into an ordered structure, we employed a structurally ordered graphene-based material to modify a phenolic resin/carbon fiber precursor and designed two composite modification structures that are straightforward to implement in processing. The internal microstructure of the composites was characterized by XRD and SEM. The results indicate that graphene oxide was converted into reduced graphene oxide during the carbonization process, which enhanced the structural order of the composites after carbonization and graphitization. The graphene based material effectively promotes the transformation of pyrolytic carbon derived from resin into an ordered graphitic microcrystalline structure, thereby enhancing the performance of the carbon/carbon composites and demonstrating a favorable structural induction effect. After graphitization treatment, the electrical conductivity and thermal conductivity of the reduced graphene oxide/carbon fiber/carbon based composite materials increased by 8.5% and 12%, respectively, compared to those of the unmodified composite.

KEYWORDS: Carbon-based composite materials; reduced graphene oxide; microstructure; electrical conductivity; thermal conductivity

1 Introduction

Carbon fiber reinforced carbon matrix (C/C) composites have gradually become the thermal structural materials for key components such as engine throat linings and missile nose tips due to their excellent ablation resistance [1]. Furthermore, their applications are extending into fields such as mechanical braking and biomedicine [2,3]. Liquid phase infiltration is one of the important methods for preparing C/C composites. Commonly used liquid precursors include pitch [4] and resins, with resin-based precursors mainly consisting of phenolic resins, furan resins, and others. The preform undergoes repeated cycles of impregnation and carbonization, followed by graphitization, to obtain C/C composites with the required density. During carbonization and graphitization, the graphitization behavior of hard carbon derived from phenolic resin is also influenced by carbonization methods such as autogenous pressure [5]. As the degree of graphitization increases, the properties of the composite material change, exhibiting a continuous improvement in thermal conductivity [6]. Resin-pyrolyzed glassy carbon is an amorphous carbon material

composed of disordered arrangement of carbon microcrystals [7]. The microcrystalline structure of glassy carbon lacks orientation in any specific direction, and its carbon layers form disordered network structures through long ribbon like stacking, making it difficult to graphitize. Consequently, this can adversely affect the properties of the C/C composite material.

Graphene oxide (GO) is a chemical derivative of graphene. It retains the basic structural framework of graphene, with various oxygen-containing functional groups—such as carboxyl, hydroxyl, and carbonyl groups—attached to some carbon atoms on the edges of graphene sheets [8]. Compared with graphene, GO contains numerous oxygen-containing functional groups, which grant it excellent dispersibility in a range of solvents, including water and ethanol. The excellent mechanical, thermal, and other physical properties of graphene have also been widely applied in the field of C/C composites [9–11]. By incorporating graphene into carbon fibers to prepare modified C/C composites, the densification rate of the composite can be increased by 10%, and its flexural strength can be enhanced by 30% [12]. By modifying carbon fiber preforms with graphene/pitch coatings and graphene aqueous solution coatings, the flexural strength of the resulting modified C/C composites was increased by as much as 150% [13]. Using a method of grafting GO onto carbon fibers, the resultant C/C composites not only achieved enhancements of 76.4% in flexural strength and 44.6% in interlaminar shear strength, but also exhibited higher thermal conductivity in the X-Y and Z directions by 13.3%–19.8% and 37.7%–176.3% respectively under conditions ranging from 50°C to 900°C. Furthermore, they demonstrated improved friction stability and reduced friction loss [14]. Reduced graphene oxide not only promotes fiber graphitization in phenolic resin-based carbon/carbon composites [15], but also forms a synergistic effect with the matrix in coal-based porous carbon composites to improve the carbon microcrystalline structure [16]. Due to the good compatibility between GO and the resin matrix, it can be well dispersed in the resin at the precursor stage and also enhance the fiber/resin interfacial bonding [17–20], which is highly beneficial for reducing internal voids/pores in carbon fiber/phenolic resin composites. The composite of GO with alumina can also improve thermal conductivity [21]. However, when reduced graphene oxide is directly used as an additive in ceramic matrices, the presence of RGO agglomerates [22] tends to increase the performance variability of the resulting composites.

As can be seen, graphene-based materials significantly enhance the performance advantages of C/C composites. However, the molding processes for such modified composites are mostly complex, presenting substantial challenges for engineering applications. Considering that when resin precursors are used to prepare C/C composites, the glassy carbon formed after pyrolysis of the resin precursors is difficult to graphitize, and the low degree of graphitization of the matrix carbon adversely affects thermophysical, mechanical, and friction and wear performance of the composites, it would be an intriguing question whether graphene-based materials could be utilized through a simple process to enhance the performance of C/C composites. We employed a simple mixture of GO and phenolic (PF) resin precursor, utilizing the characteristic of GO being transformed into a reduced graphene oxide (RGO) structure under high-temperature treatment. By using RGO, which has a higher degree of graphitization as a modifier, we investigated the influence of RGO on the microstructure of C/C composites, as well as its effects on the thermal and electric properties of the composites.

2 Materials and Methods

2.1 Preparation of Graphene Oxide (GO) Dispersion

An appropriate amount of deionized water was added to a graphene oxide (GO) hydrogel with a concentration of approximately 14 g/L, followed by ultrasonic treatment for 20 min to prepare a low-concentration GO aqueous solution. An appropriate amount of the GO aqueous solution was taken and subjected to multiple rounds of centrifugation to remove most of the water. The GO was then dispersed in

ethanol, subjected to ultrasonic treatment for 15 min, and centrifuged. This process was repeated three times to prepare a GO ethanol dispersion of a specific concentration.

2.2 Preparation of Graphene Oxide/Carbon Fiber/Phenolic Resin (GO/CF/PF) Composite Precursor

Phenolic resin (PF) and hexamethylenetetramine at 8% of its mass in were dissolved in ethanol. The required amount of GO was weighed based on mass ratios of GO to PF of 0%, 0.1%, and 0.5%. The GO ethanol dispersion was then uniformly mixed with the PF ethanol solution and subjected to ultrasonic treatment for 15 min. The carbon fabric used was W3031 plain weave fabric, from Weihai Tuozhan Fiber Co., Ltd., China. Carbon fiber prepregs were prepared using the wet process, air-dried for 24 h, and then oven-dried at 60°C for 2 h. The prepreg was placed into a mold, and the GO/CF/PF composite was fabricated using a compression molding process. The curing conditions were set as follows: 150°C/1 h + 180°C/1 h + 200°C/1 h. The temperature was raised according to these conditions for curing, followed by pressure holding and cooling to room temperature. After depressurization and demolding, the GO/CF/PF composite precursor laminate was obtained.

Directly blending GO with PF resin significantly increases the viscosity of the mixed solution, which adversely affects the prepreg process. To enhance the content of graphene-based materials in the composite, we employed a method of adding an additional coating of GO hydrogel between each layer of carbon fabric, thereby increasing the GO content in the composite. Prepregs were prepared using two methods: the direct blending method and the interlayer coating method, as illustrated in Fig. 1a and 1b, respectively.

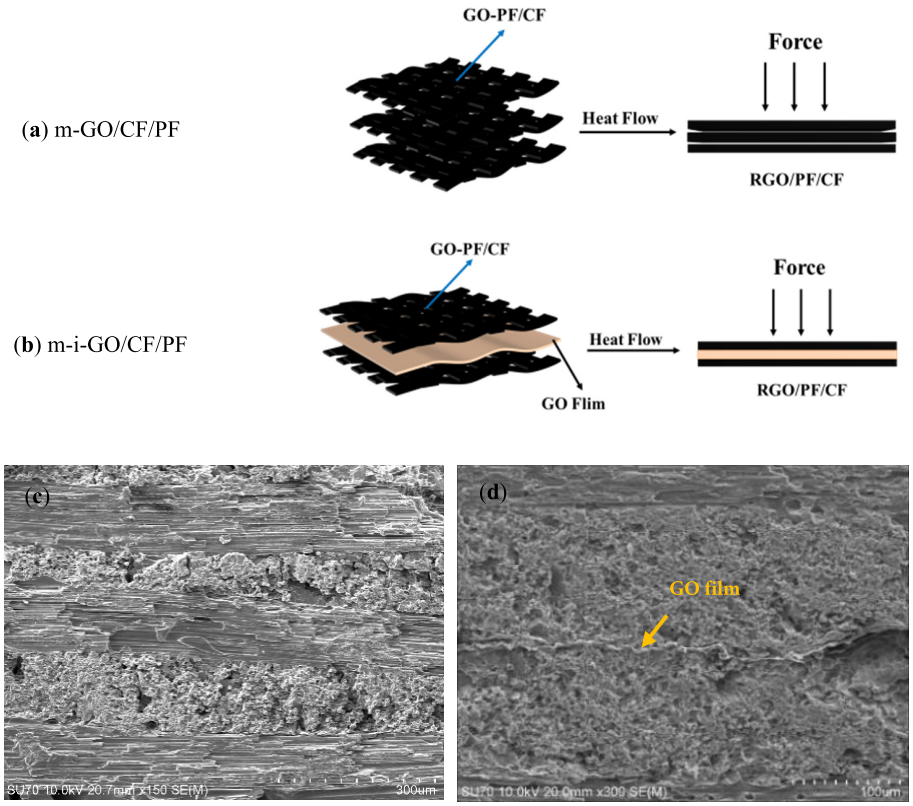

Figure 1: Schematic diagrams of the two composite structures: (**a**) mixed GO/CF/PF precursor (m-GO/CF/PF), (**b**) mixed + interlayer reinforced GO/CF/PF precursor (m-i-GO/CF/PF), and SEM images showing the internal microstructures of the composites: (**c**) m-GO/CF/PF, (**d**) m-i-GO/CF/PF. The SEM samples were cryogenically fractured in liquid nitrogen and then sputter-coated with gold.

2.3 Preparation of Carbon Fiber/Carbon (C/C) Preform

The GO/CF/PF composite precursor laminate prepared via the above compression molding process was placed in a tube furnace for carbonization under an argon atmosphere. The temperature was raised to 500°C and held for 1 h, and then further increased to 950°C and held for 2 h. After the furnace temperature dropped below 100°C, the sample was removed to obtain a C/C composite preform.

2.4 Multiple Cycles of Resin Impregnation and Carbonization of the Carbon Fiber/Carbon (C/C) Preform

We employed an impregnation method at ambient temperature and pressure. A 30% phenolic resin ethanol solution (containing hexamethylenetetramine) was used as the impregnating agent for the preform. The preform was immersed in the resin solution until fully submerged and was impregnated for 3 h by relying on the capillary pressure within the pores of the preform. Subsequently, the impregnated preform was placed in an oven and dried at 50°C for 0.5 h, completing one cycle of resin impregnation. The resin impregnated preform was placed in a tube furnace under an argon atmosphere. The temperature was raised to 500°C and held for 1 h, then further increased to 950°C for 2 h to complete one carbonization cycle. After cooling, the sample was removed. This was followed by ten repeated cycles of impregnation and carbonization, resulting in the carbonized RGO/CF/C-PF sample.

2.5 Graphitization Process of the Carbon Fiber/Carbon (C/C) Composite

The carbonized sample was placed in a high-temperature graphitization furnace (model VVG-0101, Hunan Dingli Technology Co., Ltd.) and subjected to graphitization according to the following temperature program: 500°C/1 h + 950°C/2 h + 1200°C/10 min + 1500°C/10 min + 1800°C/10 min + 2100°C/10 min + 2300°C/2 h. After cooling, when the furnace temperature dropped below 100°C, the sample was removed to obtain the graphitized RGO/CF/C-PF composite sample.

2.6 Performance Testing and Characterization of Materials

Thermal analysis tests were conducted using a DSC 204 F1 differential scanning calorimeter. The testing range was from room temperature to 325°C, with a heating rate of 10°C/min under a nitrogen atmosphere. Various thermal performance parameters were derived using the NETZSCH Proteus thermal analysis software. Thermogravimetric analysis was performed using a STA 449F3 Jupiter synchronous thermal analyzer, with the temperature ranging from room temperature to 950°C at a heating rate of 10°C/min under a nitrogen atmosphere. The crystallinity of the composites was analyzed using a D8-A25 X-ray diffractometer from Bruker (USA), with a scanning range from 5° to 90° and a step size of 0.016°. The morphology of the composites was observed using an SU-70 field emission scanning electron microscope, with the samples sputter-coated with gold. The microstructure of GO was examined using a JEOL model JEM-2100 transmission electron microscope.

The density of the composites was measured using the water displacement method and calculated according to Formula (1).

$$\rho = \frac{m}{\mathrm{v}} = \frac{m\rho_{\mathrm{w}}}{m1 - m0} \tag{1}$$

In Eq. (1): m is the dry weight of the sample (g); m_1 is the mass of the sample after immersion in water for 24 h, removal, and wiped dry with filter paper (g); m_0 is the suspended weight of the sample in water (g); ρ_w is the density of water (g·cm^{-3}).

The open porosity of the samples was tested in accordance with the ASTM C2000 [23] standard and calculated using Formula (2). The samples were placed in a beaker filled with distilled water, boiled for 2 h, cooled to room temperature, and then left to stand in water for 12 h.

$$P = \frac{M1 - M0}{M1 - M2} \tag{2}$$

In Eq. (2): P represents the open porosity; M_0 is the mass of the specimen in the dry state (g); M_1 is the mass of the saturated specimen in air (g); M_2 is the mass of the saturated specimen in water (g).

Carbon materials are composed of graphite microcrystals and amorphous carbon, with the proportion of graphite microcrystals referred to as the graphitization degree. The graphitization degree of as-manufactured C/C composites is generally below 100% due to various factors [24]. Therefore, the quality of C/C composites is evaluated by calculating their graphitization degree. The degree of graphitization of carbon materials is often assessed by calculating the interplanar spacing using the Bragg equation. The interlayer spacing (d_{002}) of carbon materials is determined based on the Bragg Eq. (3):

$$\mathrm{d002} = \frac{\lambda}{2\sin\theta} \tag{3}$$

In Eq. (3): d_{002} is the interlayer spacing of the carbon (002) crystal plane; λ is the wavelength of the X-ray (λ = 0.154178 nm); θ is the angle corresponding to the diffraction peak of the (002) crystal plane.

Based on the Franklin model [25], the simplified Formula (4) for calculating the graphitization degree is derived from the Mering-Maire formula [26]:

$$G = \frac{(0.3440 - d_{002})}{0.3440 - 0.3354} \times 100 \tag{4}$$

In Eq. (4): G represents the graphitization degree (%); 0.3440 is the interlayer spacing of completely amorphous carbon (nm); 0.3354 is the interlayer spacing of an ideal graphite crystal (nm); d_{002} is the interlayer spacing of the carbon (002) crystal plane (nm).

According to the Scherrer formula [27] (5), the crystallite stacking height Lc is calculated.

$$Lc = \frac{K\lambda}{\beta\cos\theta} \tag{5}$$

In Eq. (5): λ is the incident X-ray wavelength, which is 0.154 nm when using CuKα; d is the interplanar spacing (nm); θ is the diffraction angle (°); K is the Scherrer geometric factor, also known as the shape factor, and K = 0.89 when calculating Lc; β is the full width at half maximum (FWHM) of the diffraction peak (rad).

The Raman spectra of the samples were acquired using a confocal Raman spectrometer HR Evolution (Horiba France SAS, France) with a 532 nm laser as the excitation source. The measurements were carried out at room temperature, and the spectral acquisition range was 1000–3500 cm^{-1}. After plotting the raw Raman spectral data using Origin2024b, peak fitting analysis was performed on the characteristic peaks. Baseline correction was carried out using the user-defined baseline correction function in Origin2024b. The characteristic peaks of the D band (1380 cm^{-1}) and G band (1580 cm^{-1}) were identified for analysis. Lorentzian functions were used for peak fitting.

According to the Cancado formula [28] (6), the in-plane crystallite size La is calculated.

$$La = \frac{C}{I_D/I_G} \tag{6}$$

In Eq. (6), I_D/I_G is the intensity area ratio of the *D* band (1350 cm^{-1}) to the *G* band (1580 cm^{-1}) in the Raman spectrum; *C* is a laser wavelength-dependent constant, and *C* is taken as 19.2 nm when the excitation wavelength is 532 nm.

The electrical conductivity of the composites was measured using an RTS-9 four-probe tester at room temperature in the in-plane direction of the samples. The samples had smooth and flat surfaces with uniform thickness, and the average value was taken from five measurements. The thermal conductivity of the composites was determined using the heat flow method with a DRL-III thermal conductivity tester. The sample surfaces were ground and polished, and the sample dimensions were 20 mm × 20 mm. Thermal conductivity was measured in the in-plane direction of the samples. For each sample, an average of five measurements were tested, and the mean value was taken.

3 Results and Discussion

3.1 The Two Designed Precursor Materials for GO-Modified Carbon-Based Composites

The pyrolytic carbon of phenolic resin is difficult to transform into a graphite structure during carbonization and graphitization processes. We anticipate that the ordered lamellar structure of graphene-based materials can promote the structural transformation of resin-derived pyrolytic carbon toward the crystalline structure of graphite, thereby enhancing the regularity of its structure. We used GO as a modifying material for CF/PF and designed two modified structures as precursors for carbon-based composites. One structure involves uniformly mixing GO with phenolic resin to serve as a composite resin matrix, which infiltrates the carbon fibers to form a GO/CF/PF precursor. The schematic of this structure is shown in Fig. 1a (mixed GO/CF/PF precursor, designated as m-GO/CF/PF). The other structure entails depositing a GO film onto the carbon fabric, followed by impregnating the fabric with a GO-PF composite matrix. This approach increases the GO content in the precursor, with the total GO content reaching 0.5%. The schematic of this structure is illustrated in Fig. 1b (mixed + interlayer reinforced GO/CF/PF precursor, designated as m-i-GO/CF/PF). The second structural design was developed to both increase the GO content in the precursor and avoid significantly raising the processing difficulty of the composite resin impregnating the carbon fibers. Subsequently, composites were fabricated using these two structures. The internal microstructures of these two composites are shown in Fig. 1c,d. Among them, m-i-GO/CF/PF features an additional GO layer between the carbon fabric layers compared to m-GO/CF/PF.

During this process, we utilized GO hydrogel, and the microstructure of GO is shown in Fig. 2. From the TEM image in Fig. 2a, the sheet-like structure of GO can be observed, appearing translucent with thin layers and a low number of stacked sheets. The SEM image in Fig. 2b reveals a large number of wrinkled, sheet-like structures in GO. We analyzed the Raman spectrum of GO (Fig. 2c), in which 1352 cm^{-1} is the D band of GO, 1595 cm^{-1} is the G band of GO, and the I_D/I_G ratio is 1.73.

Following the carbonization process for GO/CF/PF precursors, under argon protection, the temperature was raised to 500°C and held for 1 h, then further increased to 950°C and maintained for 2 h to complete one cycle of carbonization. X-ray diffraction (XRD) analysis was conducted on GO and its products obtained after the carbonization process. From the XRD curve in Fig. 2d, it can be observed that graphite exhibits a high-intensity diffraction peak at the carbon (002) crystal plane, specifically at 2θ = 26.5°. Using the Bragg equation, the calculated interplanar spacing is approximately 0.340 nm, indicating that the crystalline structure of graphite is highly ordered. The diffraction peak corresponding to the carbon (002) crystal plane of GO disappears, indicating a decrease in its crystallinity. The structure of GO transforms from an ordered layered configuration into exfoliated sheets. The characteristic diffraction peak of GO appears at 2θ = 10.3°, corresponding to an interlayer spacing of approximately 0.77 nm. This increase in layer

spacing is primarily attributed to the presence of oxygen-containing functional groups such as –COOH and –C=O, which disrupt the regular stacking of graphene layers, introduce more crystal defects, and ultimately lead to the enlarged interlayer spacing of GO [29]. After the material sample was heat-treated at 950°C, the characteristic (001) diffraction peak of GO disappeared. The thermal reduction of GO resulted in the formation of RGO, which was manifested by the broadening and weakening of the diffraction peak corresponding to the carbon (002) crystal plane, with the peak position shifting to approximately 25°. The residual oxygen-containing functional groups on the surface of RGO and the wrinkles formed by RGO to reduce surface energy result in less ordered stacking of RGO sheets, larger interlayer spacing compared to graphite, and poorer crystallinity. The results show that GO gradually converts into RGO during the carbonization process of the precursor. Accordingly, the carbonized composites are designated as m-RGO/CF/C-PF and m-i-RGO/CF/C-PF, respectively.

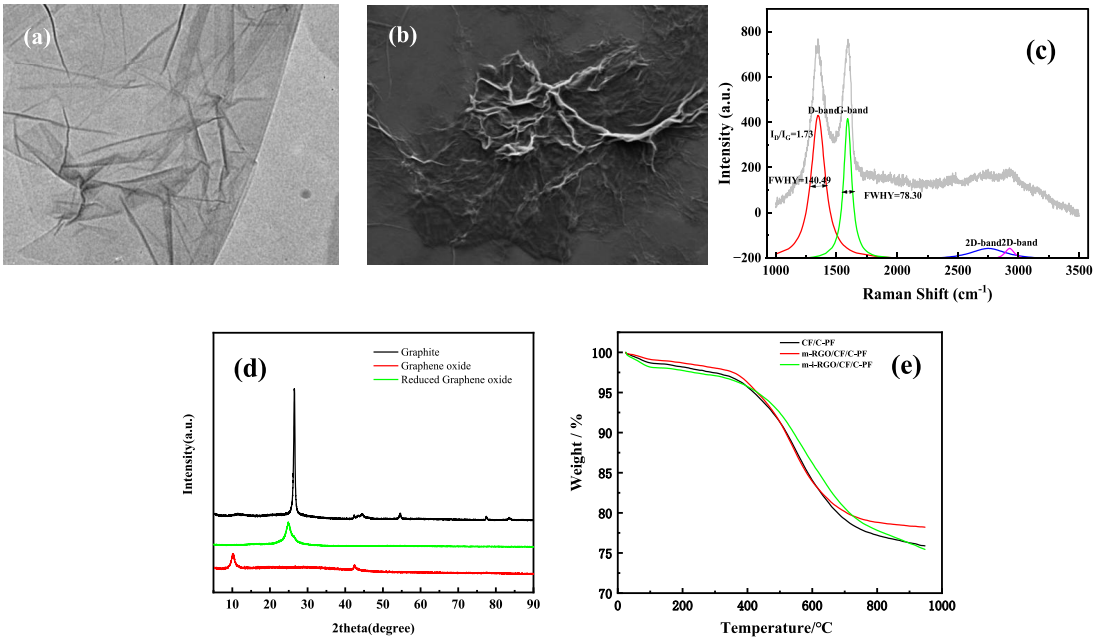

Figure 2: Microstructure of graphene oxide: (**a**) TEM image, (**b**) SEM image, and (**c**) Raman spectrum; XRD patterns of graphite, GO, and RGO (**d**); and thermogravimetric curve of RGO/CF/PF (**e**). The colored curves in Fig. 2c are the fitting curves.

After modification with GO, the precursors also demonstrated improved high-temperature carbonization performance. As shown in Fig. 2e, the residual mass of PF at 950°C was 75.9%, while that of m-GO/PF reached 78.2%, and m-i-GO/PF showed a residual mass of 76.3% at the same temperature.

3.2 Carbonization of Composites

The composites were further subjected to multiple cycles of impregnation and carbonization to obtain the carbonized composites. During the carbonization process of the precursors, a large amount of pyrolytic products are released, resulting in the formation of numerous pores within the material, including both open and closed pores [30]. Typically, repeated impregnation and carbonization cycles can be employed to fill the open pores formed during pyrolysis, thereby enhancing the overall density of the composites. Fig. 3 shows the internal microstructures of RGO/CF/C-PF after 1, 3, 5, and 7 cycles of impregnation and carbonization. As shown in Fig. 3, after only one carbonization cycle, the sample exhibits relatively large internal pores, along

with delamination between the fiber bundles and the matrix (Fig. 3a). After three cycles of carbonization, the delamination between the fiber bundles and the matrix in the sample decreased significantly, although larger pores still remained (Fig. 3b). Following five carbonization cycles, the average pore size of the sample continued to decrease (Fig. 3c). After seven carbonization cycles, the larger pores inside the sample were largely filled (Fig. 3d). Although some smaller pores still existed on the surface, the density of the composite increased substantially with the number of carbonization cycles.

Fig. 3e illustrates the density changes of RGO/CF/C-PF during the cyclic carbonization process. As the number of impregnation and carbonization cycles increases, the density of RGO/CF/C-PF shows an upward trend. This is primarily due to the gradual filling of internal pores in the composite material by the matrix carbon formed from the resin during carbonization, which reduces the internal porosity and progressively increases the density. As the number of carbonization cycles increases, the increment in density gradually decreases and tends to level off. Combined with Fig. 3d, it can be seen that with more carbonization cycles, the internal densification of the composite material improves, and the pore size gradually decreases. Simultaneously, the surface tension of the open pores also increases accordingly. At this stage, due to the increased surface tension in the pores, the resistance to resin impregnation becomes greater, leading to reduced impregnation efficiency. As a result, it becomes difficult to further increase the density of the composite material [31].

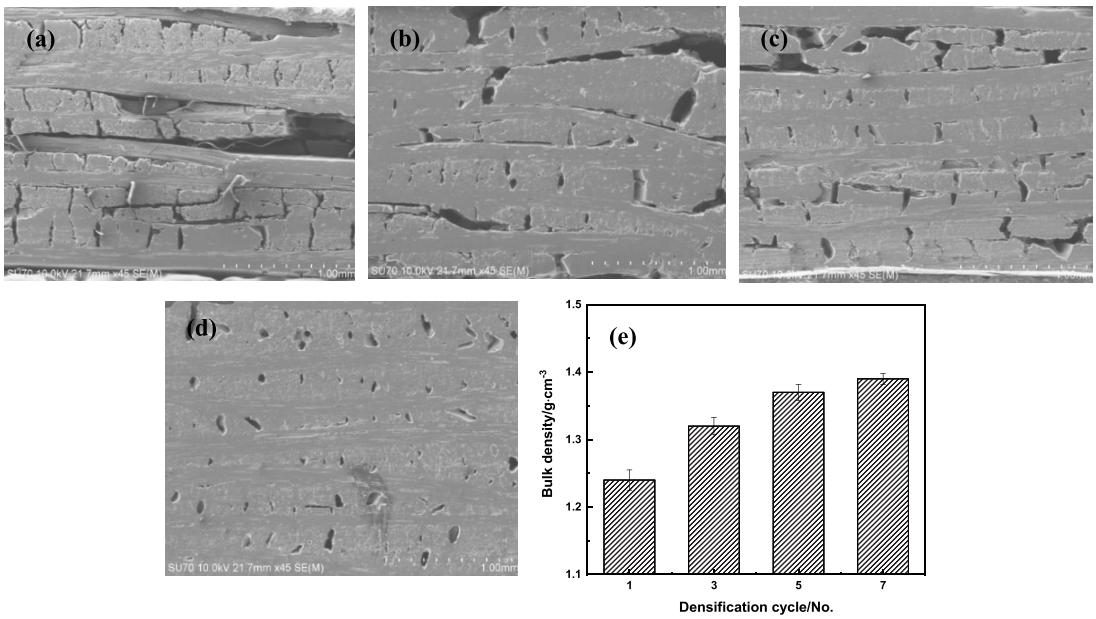

Figure 3: Internal microstructures of RGO/CF/C-PF: (**a**) after one impregnation-carbonization cycle; (**b**) after three impregnation and carbonization cycles; (**c**) after five impregnation and carbonization cycles; (**d**) after seven impregnation and carbonization cycles; and (**e**) changes in the density of the composite material with the number of carbonization cycles. The SEM samples were cryogenically fractured in liquid nitrogen and then sputter-coated with gold.

Fig. 4 presents the internal microstructures of the corresponding composites. The results in Fig. 4a (CF/C-PF) exhibit the formation of certain microcrystalline structures. In contrast, Fig. 4c (m-RGO/CF/C-PF) displays a relatively ordered microcrystalline morphology internally, with some of the resin-derived carbon around the fiber bundles showing a banded structure. Additionally, a small amount of ordered graphite microcrystalline structures can be observed. This is because during the carbonization process, RGO sheets adhere to the surface of the fiber bundles, and the resin-derived carbon grows around these bundles.

At this stage, the RGO sheets act as nucleation sites for the matrix carbon at the interface, inducing the formation of oriented, ribbon-like grains in the matrix carbon, thereby promoting its crystallization. A certain degree of microcrystalline structure has also formed inside m-i-RGO/CF/C-PF (Fig. 4e). Overall, RGO uniformly distributed within the resin-derived carbon is more effective in inducing the formation of ordered structures in resin-derived pyrolytic carbon. In contrast, although the amount of RGO between the fiber layers is relatively larger (approximately 0.4%), the actual contact area between this interlayer RGO and the resin-derived pyrolytic carbon is much smaller than that of the uniformly distributed RGO. As a result, the interlayer RGO has a less pronounced effect on inducing ordered structures in the resin-derived carbon.

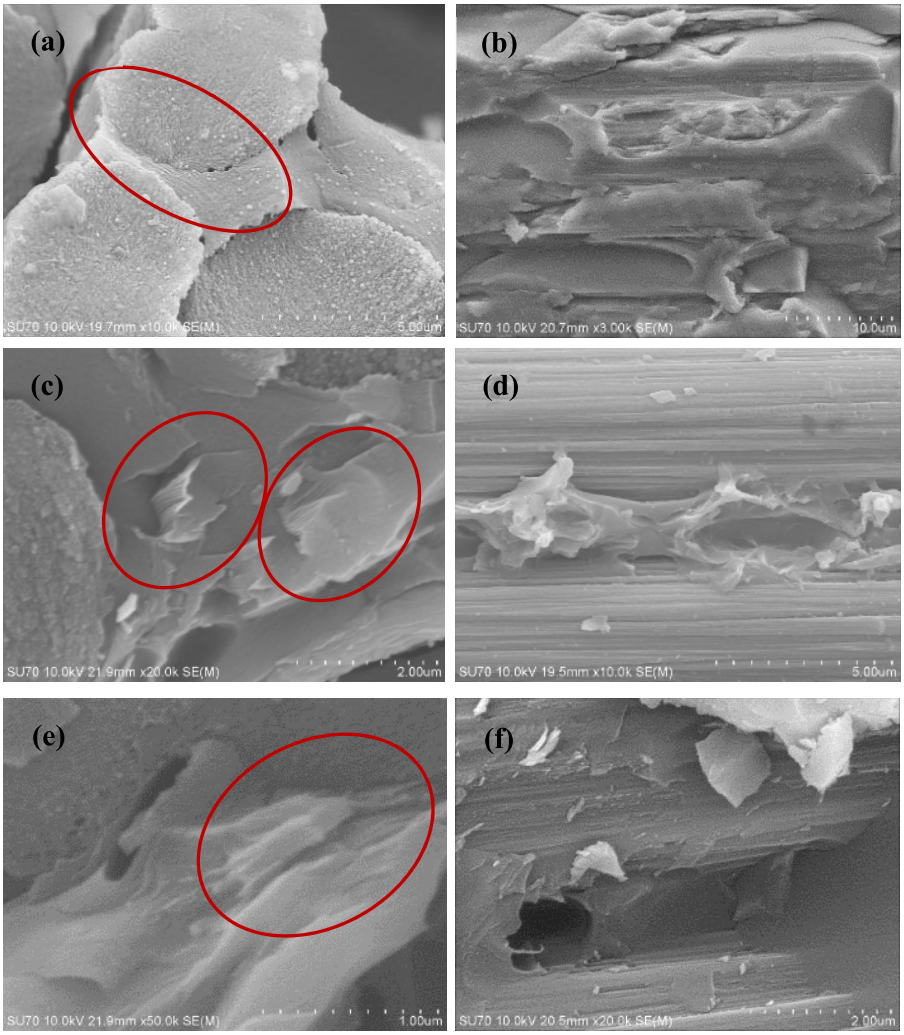

Figure 4: SEM images of the carbonized composites microstructures: (**a**,**b**) CF/C-PF; (**c**,**d**) m-RGO/CF/C-PF; (**e**,**f**) m-i-RGO/CF/C-PF. The SEM samples were cryogenically fractured in liquid nitrogen and then sputter-coated with gold. The red ellipses indicate the ordered crystalline structure.

Additionally, in CF/C-PF, the resin-derived carbon within the fiber bundles fills around the bundles, and the bonding between the fibers and the resin-derived carbon is good. However, a small number of pores still exist at the interface between the fiber bundles and the matrix carbon (Fig. 4b). In m-RGO/CF/C-PF, the RGO and CF form a relatively tight interface (Fig. 4d). For m-i-RGO/CF/C-PF (Fig. 4f), the GO layer between the fiber layers likely hindered the flow and infiltration of the blended composite resin GO-PF within

the interlayer regions, which adversely affected the internal homogeneity of the composite material and increased its porosity/void content. Based on the open porosity results of the composites after carbonization presented in Table 1, m-RGO/CF/C-PF shows lower open porosity than CF/C-PF, while m-i-RGO/CF/C-PF exhibits higher open porosity than CF/C-PF. The results show that the RGO film layer between the carbon fiber layers likely had a negative impact on resin flow during the impregnation and molding processes of the composites. Consequently, m-RGO/CF/C-PF achieves a relatively higher density among the three materials. When the porosity of a material is low and its compactness increases, the density of the material increases, which enhances its electrical and thermal conductivity. Conversely, increased porosity reduces the electrical and thermal conductivity of the composite material [32]. The porosity of m-RGO/CF/C-PF is lower than that of m-i-RGO/CF/C-PF, and the density of the former is higher than that of the latter, which benefits the improvement of the electrical and thermal conductivity of m-RGO/CF/C-PF.

Table 1: Density and open porosity of the carbonized composites.

Samples	Density/g·cm^{-3}	Open Porosity/%
CF/C-PF	1.51 ± 0.012	10.2
m-RGO/CF/C-PF	1.53 ± 0.009	9.0
m-i-RGO/CF/C-PF	1.50 ± 0.011	11.3

Fig. 5a shows the XRD pattern of the composite material after 10 cycles of impregnation and carbonization. The diffraction peak of the carbon (002) crystal plane is a characteristic peak used to evaluate the degree of graphitization in carbon materials. As seen in Fig. 5a, CF/C-PF exhibits a broad, low-intensity, broad and diffuse diffraction peak around $2\theta = 25°$, indicating that the crystallinity of this sample is relatively low. After modification with GO, the crystallinity of the carbonized composites changed. The peak of m-RGO/CF/C-PF became narrower compared to that of CF/C-PF, indicating higher crystallinity. However, the crystallinity of m-i-RGO/CF/C-PF was closer to that of CF/C-PF and lower than that of m-RGO/CF/C-PF. Based on the analysis of the full width at half maximum (FWHM), the FWHM of m-RGO/CF/C-PF is also smaller than that of the other two composite materials. This is because the RGO sheets in m-RGO/CF/C-PF are closely bonded with the resin. During the carbonization process, the resin-derived pyrolytic carbon arranges itself along the RGO sheet skeleton, thereby promoting the crystallization process of the resin-derived pyrolytic carbon. In m-i-RGO/CF/C-PF, an additional GO film layer was introduced between the carbon fabrics, which affected the impregnation of the composite resin (GO-PF) into the carbon fibers. As a result, the amount of GO within the carbon fiber layers was actually reduced, thereby influencing the crystallinity of the resin-derived carbon.

3.3 Graphitization of Composites

Fig. 5b shows the XRD patterns of the graphitized composites obtained after heat-treating the carbonized composites at 2300°C. Compared with Fig. 5a, it can be seen that after the 2300°C treatment, both m-RGO/CF/C-PF and m-i-RGO/CF/C-PF exhibit increased intensity of the (002) diffraction peak, a significant improvement in peak symmetry, and a shift of the diffraction angle from about 25° to 26.5°. Combined with the interplanar spacing and graphitization degree of the graphitized composites shown in Table 2, it can be seen that the interplanar spacings of both m-RGO/CF/C-PF and m-i-RGO/CF/C-PF are relatively low, far smaller than that of completely amorphous carbon (0.3440 nm) [33]. Among them, m-RGO/CF/C-PF has the smallest interplanar spacing at 0.3375 nm and a graphitization degree of 75.6%, which is significantly higher than that of CF/C-PF (68.6%). Meanwhile, m-i-RGO/CF/C-PF achieves a

graphitization degree of 70.9% after graphitization treatment, also exceeding that of CF/C-PF (Table 2). The m-RGO/CF/C-PF and m-i-RGO/CF/C-PF also exhibit larger crystallite L_a (in-plane crystallite size) and L_c (Stacking height) compared to CF/C-PF, which further contributes to the improvement of the composite's electrical and thermal conductivity [32].

Fig. 5d–f show the Raman spectra of the composites after graphitization. The peak near 1350 cm^{-1} corresponds to the D band, and the peak near 1580 cm^{-1} corresponds to the G band. From the results in Fig. 5, the G band of the RGO-modified composites becomes significantly sharper with a narrower full width at half maximum (FWHM), and the area of the G band is also notably larger than that of CF/C-PF. Specifically, the I_D/I_G of CF/C-PF is 5.02 (Fig. 5d), that of m-RGO/CF/C-PF is 0.30 (Fig. 5e), and that of m-i-RGO/CF/C-PF is 1.38 (Fig. 5f). Compared to CF/C-PF, the narrower FWHM of the G band, the sharper crystalline band shape, and the lower I_D/I_G of the RGO-modified composites indicate that the crystallinity of the modified composites is improved. Among them, the effect is more pronounced for m-RGO/CF/C-PF. The results show that RGO enhances ordered crystallization, thus increasing the overall graphitization degree of the material.

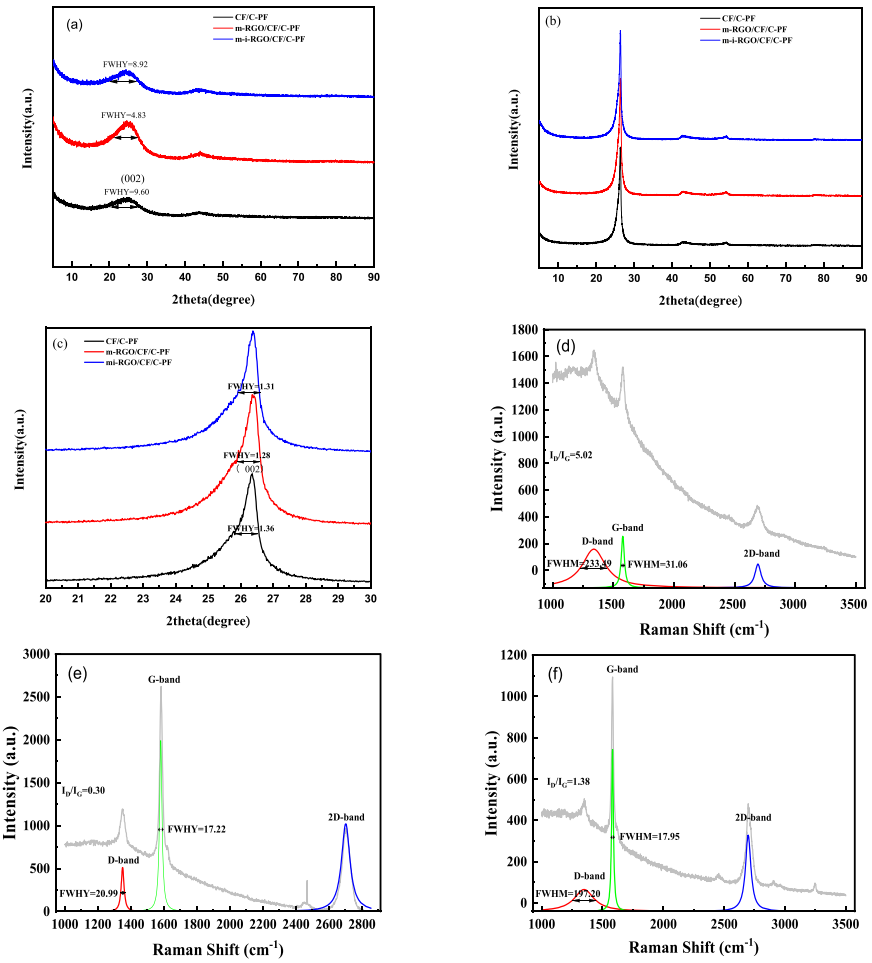

Figure 5: XRD patterns of the composites after carbonization (**a**) and graphitization at 2300°C (**b**), locally magnified view of the diffraction angle from 24° to 30° after graphitization (**c**), and Raman spectra of the composites after graphitization at 2300°C, (**d**) CF/C-PF, (**e**) m-RGO/CF/C-PF, (**f**) m-i-RGO/CF/C-PF. The colored curves in Fig. 5d–f are the fitting curves.

Table 2: Crystallite size and graphitization degree of the graphitized composites.

Samples	Interplanar Spacing/nm	In-Plane Crystallite Size (L_a)/nm	Stacking Height (L_c)/nm	Graphitization Degree/%
CF/C-PF	0.3381	3.82	5.90	68.6%
m-RGO/CF/C-PF	0.3375	64.00	6.30	75.6%
m-i-RGO/CF/C-PF	0.3379	13.91	6.16	70.9%

From the internal microstructures of the graphitized composites shown in Fig. 6, it can be seen that after graphitization at 2300°C, the CF/C-PF composite develops a more ordered internal structure compared to the state after carbonization (Fig. 6a,b). In m-RGO/CF/C-PF, the resin-derived carbon between the carbon fibers forms a well-ordered structure (Fig. 6c). Additionally, the resin-derived carbon adhered to the RGO surface covering the carbon fiber also clearly exhibits a certain degree of ordered regularity (Fig. 6d). The m-i-RGO/CF/C-PF also displays a similarly ordered and regular morphology comparable to that of m-RGO/CF/C-PF (Fig. 6e,f). The results show that RGO significantly induces the ordering and regularity of the surrounding resin-derived carbon, thereby enhancing the graphitization degree of both m-RGO/CF/C-PF and m-i-RGO/CF/C-PF. However, in m-i-RGO/CF/C-PF, the RGO film between the carbon fabric layers is difficult to impregnate with resin, so almost no resin-derived carbon is observed within the RGO film after graphitization. Furthermore, during graphitization, RGO undergoes further removal of non-carbon atoms, which tends to create voids/pores within the RGO film. This also reduces the effectiveness of the RGO in the film for inducing crystallization.

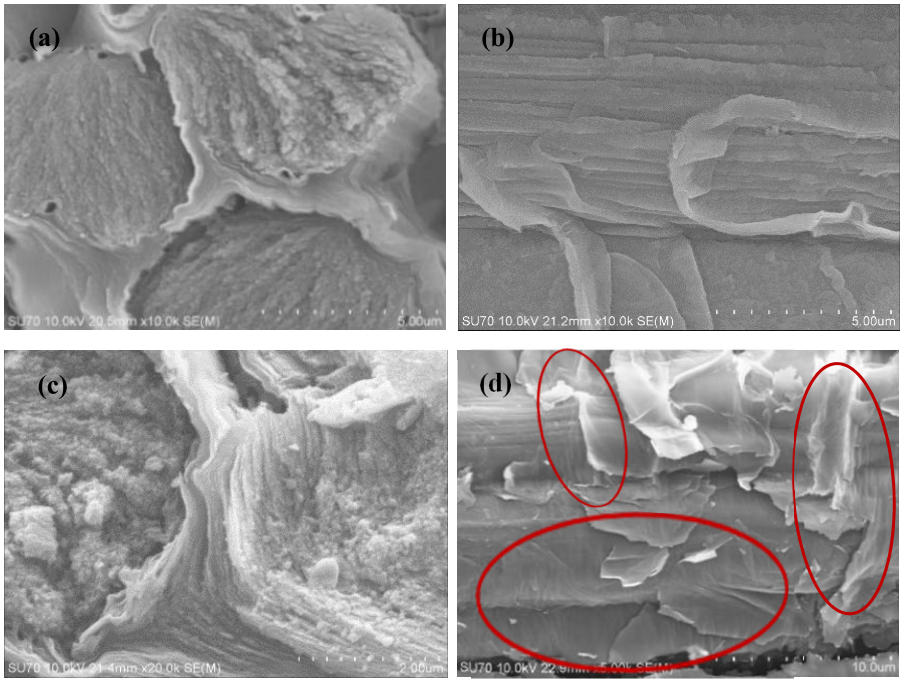

Figure 6: (Continued)

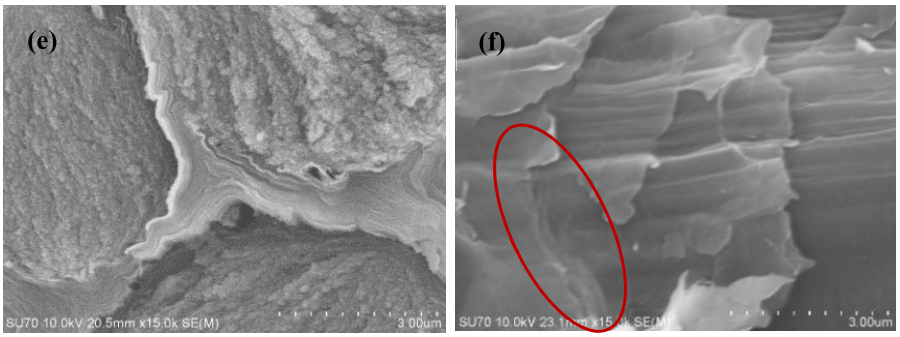

Figure 6: SEM images of the internal microstructures of the graphitized composites: (**a**,**b**) CF/C-PF; (**c**,**d**) m-RGO/CF/C-PF; (**e**,**f**) m-i-RGO/CF/C-PF. The SEM samples were cryogenically fractured in liquid nitrogen and then sputter-coated with gold. The red ellipses in Fig. 6d,f indicate the ordered crystalline structure.

3.4 Performance of the Composites

The electrical conductivity and thermal conductivity of the composites after carbonization and graphitization were tested separately, and the results are shown in Table 3. After carbonization, compared with CF/C-PF, both m-RGO/CF/C-PF and m-i-RGO/CF/C-PF show significant improvements in electrical conductivity and thermal conductivity. The electrical conductivity of the carbonized m-RGO/CF/C-PF and carbonized m-i-RGO/CF/C-PF increased by 18.1% and 11.3%, respectively, compared with that of carbonized CF/C-PF. Meanwhile, the thermal conductivity of the carbonized m-RGO/CF/C-PF and carbonized m-i-RGO/CF/C-PF improved by 36.1% and 25.7%, respectively, compared with that of carbonized CF/C-PF, demonstrating a more pronounced enhancement in thermal performance.

Table 3: Properties of carbonized and graphitized composites.

Samples		CF/C-PF	m-RGO/CF/C-PF	m-i-RGO/CF/C-PF
Electrical conductivity/ ($S \cdot cm^{-3}$)	Carbonization	107.0 (+5.9, −5.1)	126.4 (+6.8, −4.6)	119.1 (+7.6, −5.1)
	Average increase	/	18.1%	11.3%
	Graphitization	196.5 (+5.8, −6.5)	213.3 (+7.4, −6.3)	206.7 (+11.3, −10.6)
	Average increase	/	8.5%	5.2%
Thermal conductivity/ ($W \cdot m^{-1} \cdot K^{-1}$)	Carbonization	1.44 (+0.23, −0.32)	1.96 (+0.25, −0.33)	1.81 (+0.43, −0.32)
	Average increase	/	36.1%	25.7%
	Graphitization	5.75 (+0.34, −0.26)	6.44 (+0.41, −0.27)	6.15 (+0.24, −0.12)
	Average increase	/	12%	7%

After graphitization, the electrical conductivity of the graphitized m-RGO/CF/C-PF and graphitized m-i-RGO/CF/C-PF increased by 8.5% and 5.2%, respectively, compared with that of graphitized CF/C-PF. Meanwhile, the thermal conductivity of the graphitized m-RGO/CF/C-PF and graphitized m-i-RGO/CF/C-PF improved by 12% and 7%, respectively, compared with that of graphitized CF/C-PF. The results show that both the electrical and thermal conductivities of the carbonized composites and graphitized composites have been significantly improved through the application of RGO modification.

4 Conclusion

In order to enhance the transformation of glassy carbon formed from the pyrolysis of resin into ordered graphite microcrystals during the preparation of carbon/carbon (C/C) composites from carbon fiber/phenolic resin (CF/PF) precursors, a simple, facile, and low-cost compression molding method was applied to modify the phenolic resin/carbon fiber precursor using graphene-based materials. Two modification structures with straightforward processing routes were designed. One is the modified composite obtained by blending graphene oxide (GO) with phenolic resin (m-GO/CF/C-PF), and the other is the composite produced by adding an extra layer of GO between the carbon fabric plies to increase the GO content in the material (m-i-GO/CF/C-PF). The results show that GO was converted into reduced graphene oxide (RGO) during the carbonization process. During both carbonization and graphitization, RGO demonstrated a favorable structural induction effect, enhancing the structural orderliness within the composites. The amount of ordered graphite microcrystals in the composites increased significantly, and the degree of graphitization was improved. As a result, both the carbonized and graphitized composites exhibited a notable enhancement in electrical and thermal conductivity. After graphitization treatment, the graphitization degree of m-RGO/CF/C-PF increased from 68.6% (for CF/C-PF) to 75.6%, while its electrical conductivity and thermal conductivity improved by 8.5% and 12%, respectively, compared to CF/C-PF. Although m-i-RGO/CF/C-PF has a higher overall RGO content, the actual contact area between the interlayer RGO and the resin-derived pyrolytic carbon is limited, resulting in a weaker modification effect than that of m-RGO/CF/C-PF. Nevertheless, m-i-RGO/CF/C-PF still enhanced the electrical and thermal conductivity of the graphitized composite by 5.2% and 7%, respectively, relative to CF/C-PF.

Acknowledgement: The authors thank Hunan Dingli Technology Co., Ltd. for their kind sponsorship in providing the use of the VVG-0101 high-temperature graphitization furnace for the high-temperature graphitization treatment of the materials.

Funding Statement: The authors acknowledge the financial support from National Key Research and Development Program of China (2023YFB2504600), Hainan Province Science and Technology Special Fund (ZDYF2024GXJS033), Yibin City Bidding for Leadership Project (JB2024005), and State Key Laboratory of Advanced Forming Technology and Equipment Open Fund (SKL2020002).

Author Contributions: The authors confirm contribution to the paper as follows: research conception and design: Mingwei Ren, Kewei Gao, Yunbo Chen, Xiaolan Hu; experiments: Mingwei Ren, Xiangchi Hou, Hong Qiu; results and analysis: Mingwei Ren, Xiangchi Hou, Yujing Zhou, Xiaolan Hu; manuscript preparation: Mingwei Ren, Xiangchi Hou, Xinyang Peng, Yujing Zhou, Hua Bai, Xiaolan Hu; funding acquisition: Mingwei Ren, Yujing Zhou. All authors reviewed and approved the final version of the manuscript.

Availability of Data and Materials: The authors confirm that the data supporting the findings of this study are available within the article.

Ethics Approval: Not applicable.

Conflicts of Interest: The authors declare no conflicts of interest.

References

1. Zhang X, Guo L, Liu H, Zhang Y, Fu Q, Yin X, et al. Advanced anti-ablation C/C composites: structural design strategies and future perspective. Mater Today. 2024;80(2019):710–36. doi:10.1016/j.mattod.2024.09.004.
2. Bevilacqua M, Babutskyi A, Chrysanthou A. A review of the catalytic oxidation of carbon–carbon composite aircraft brakes. Carbon. 2015;95(1):861–9. doi:10.1016/j.carbon.2015.08.100.

3. Windhorst T, Blount G. Carbon-carbon composites: a summary of recent developments and applications. Mater Des. 1997;18(1):11–5. doi:10.1016/s0261-3069(97)00024-1.
4. Zang X, Dong Y, Jian C, Ferralis N, Grossman JC. Upgrading carbonaceous materials: coal, tar, pitch, and beyond. Matter. 2022;5(2):430–47. doi:10.1016/j.matt.2021.11.022.
5. Ike S, Vander Wal R. Effect of carbonization methods on graphitization of soft and hard carbons. Carbon Trends. 2024;16:100382. doi:10.1016/j.cartre.2024.100382.
6. Zhao J, Li K, Li H, Li A, Xi C. Research on the thermal conductivity of C/C composites. Acta Aeronaut Astronaut. 2005;26(4):501–4. (In Chinese). doi:10.3321/j.issn:1000-6893.2005.04.025.
7. Tzeng SS, Chr YG. Evolution of microstructure and properties of phenolic resin-based carbon/carbon composites during pyrolysis. Mater Chem Phys. 2002;73(2–3):162–9. doi:10.1016/s0254-0584(01)00358-3.
8. Lee DW, De Los Santos VL, Seo JW, Felix LL, Bustamante DA, Cole JM, et al. The structure of graphite oxide: investigation of its surface chemical groups. J Phys Chem B. 2010;114(17):5723–8. doi:10.1021/jp1002275.
9. Liu Z, Yang X, Zuo Y, Zhang X, Yan Q, Huang Q. Effects of interlaminar modification on mechanical, thermal conductivity and ablative performance of C/C composites doped with high thermal conductivity graphite film. Diam Relat Mater. 2024;145(1):111092. doi:10.1016/j.diamond.2024.111092.
10. Lee KJ, Lee MC, Shih YH, Lin HY. Doping effects of carbon nanotubes and graphene on the flexural properties and tribological performance of needle-punched carbon/carbon composites prepared by liquid-phase impregnation. Nanomater. 2023;13(19):2686. doi:10.3390/nano13192686.
11. Song S, Li X, Shen C, Li M, Hu X, Jin Z, et al. Graphene-modified C/C composites for enhanced directional thermal conductivity. J Mater Res Technol. 2025;36(6–7):4043–52. doi:10.1016/j.jmrt.2025.04.089.
12. Zhu D, Zhou K, Wu J, Huang Q, Chen T. Effects on preparation and mechanical properties of carbon/carbon composites by adding graphene in preform. Met Mater Metall Eng. 2015;(3):3–6. (In Chinese).
13. Mu C. Interface modification of carbon/carbon composite by graphene coating [dissertation]. Harbin, China: Harbin Institute of Technology; 2012. (In Chinese).
14. Yang W, Luo R, Hou Z. Effect of interface modified by graphene on the mechanical and frictional properties of carbon/graphene/carbon composites. Materials. 2016;9(6):492. doi:10.3390/ma9060492.
15. Zhang H, Gao X, Li H, Wu W, Sun S. Effect of graphene oxide on tensile and flexural properties of carbon/glass hybrid fiber-reinforced polymer composite. Polym Compos. 2021;42(10):5348–60. doi:10.1002/pc.26228.
16. Zhu H, Ren F, Pan H, Tian L, Wang T, Yu J, et al. Nitrogen-doped coal-based porous carbon and reduced graphene oxide composites for high-performance symmetrical supercapacitors. New J Chem. 2025;49(26):11509–19. doi:10.1039/d5nj01042j.
17. Liu S, Zhang J, Fan X, Hu L, Guan J, Zeng S. Enhanced mechanical, thermal properties and thermal conductivities of epoxy composites via incorporating graphene oxide-grafted carbon nanotubes hybrids. Polym Compos. 2024;45(17):15637–48. doi:10.1002/pc.28857.
18. Ma Y, Zhao Y, Li F, Xu Y, Wei X, Chen Y, et al. Influence of graphene oxide content on the morphology and properties of carbon fiber/epoxy composites. Polym Compos. 2021;42(10):5574–85. doi:10.1002/pc.26248.
19. Lyu X, Cui B, Yang X, Zhao D. Study on preparation and mechanical properties for graphene oxide/epoxy resins adhesives. J Polym Res. 2025;32(8):296. doi:10.1007/s10965-025-04527-5.
20. Qiu B, Zhang X, Xia S, Sun T, Ling Y, Zhou S, et al. Magnetic graphene oxide/carbon fiber composites with improved interfacial properties and electromagnetic interference shielding performance. Compos Part A Appl Sci Manuf. 2022;155(5):106811. doi:10.1016/j.compositesa.2022.106811.
21. Lee N, Park J, Jang N, Lee S, Kim D, Yun S, et al. Promoting thermal conductivity of alumina-based composite materials by systematically incorporating modified graphene oxide. Crystals. 2024;14(6):490. doi:10.3390/cryst14060490.
22. Broniszewski K, Woźniak J, Cygan T, Moszczyńska D, Olszyna A. Mechanical properties of silicon carbide composites reinforced with reduced graphene oxide. Materials. 2024;17(13):3370. doi:10.3390/ma17133370.
23. ASTM C20-00. Standard test methods for apparent porosity, water absorption, apparent specific gravity, and bulk density of burned refractory brick and shapes by boiling water. West Conshohocken, PA, USA: ASTM; 2015. p. 1–3.

24. Li C, Ma B, Huo X. Characterization of graphitization degree in C/C composites. New Carbon Mater. 1999;14(1):19–25. (In Chinese).
25. Franklin RE. The structure of graphitic carbons. Acta Cryst. 1951;4(3):253–61. doi:10.1107/s0365110x51000842.
26. Ishikawa T. New carbon industry. In: Lu YJ, translator, Cheng HS, editors. Harbin, China: Harbin Institute of Technology Press; 1990. (In Chinese).
27. Patterson AL. The scherrer formula for X-ray particle size determination. Phys Rev. 1939;56(10):978–82. doi:10.1103/physrev.56.978.
28. Cançado LG, Takai K, Enoki T, Endo M, Kim YA, Mizusaki H, et al. General equation for the determination of the crystallite size La of nanographite by Raman spectroscopy. Appl Phys Lett. 2006;88(16):163106. doi:10.1063/1.2196057.
29. Surekha G, Krishnaiah KV, Ravi N, Padma Suvarna R. FTIR, Raman and XRD analysis of graphene oxide films prepared by modified Hummers method. J Phys Conf Ser. 2020;1495(1):012012. doi:10.1088/1742-6596/1495/1/012012.
30. Tolbin AY, Spitsyn BV, Serdan AA, Averin AA, Malakho AP, Kepman AV, et al. Pyrolytic densification of porous carbon-carbon composite materials. Inorg Mater. 2013;49(1):49–56. doi:10.1134/S0020168512120060.
31. Zhang Z, Zhao P, Sun G, Li H, Yu P, Xie J, et al. Effect of concentration of phenolic resin on impregnation efficiency of carbon/carbon composites prepared by liquid impregnation-carbonization method. J Solid Rocket Technol. 2019;42(6):771–8. (In Chinese). doi:10.7673/j.issn.1006-2793.2019.06.016.
32. Kultayeva S, Ha JH, Malik R, Kim YW, Kim KJ. Effects of porosity on electrical and thermal conductivities of porous SiC ceramics. J Eur Ceram Soc. 2020;40(4):996–1004. doi:10.1016/j.jeurceramsoc.2019.11.045.
33. Kim JI, Jang JW, Umehara N, Jang YJ. Counterpart-dependent friction and wear of hydrogenated tetrahedral amorphous carbon under ultra-high vacuum. Carbon. 2025;238:120223. doi:10.1016/j.carbon.2025.120223.